Fatigue analysis of coil springs in the primary suspension of a railway vehicle based on synthetic spectrum for time-varying vibration load

Tengfei Wang[1], Jinsong Zhou[1], Wenjing Sun[1,] *, David Thompson[2], Zhanfei Zhang[1], Qiushi Wang[1]

[1]*Institute of Rail Transit, Tongji University, Shanghai 201804, People's Republic of China*

[2]*Institute of Sound and Vibration Research, University of Southampton, Southampton SO17 1BJ, UK*

*Corresponding author: Wenjing Sun; Email address: sunwenjing19@gmail.com

Abstract: The fatigue life of coil springs is usually predicted with a stationary Gaussian vibration load and deterministic structural parameters. However, the obtained fatigue life is inconsistent with the observed fatigue life of fractured springs which varies within a wide range. The work aims to propose a method to predict the fatigue life of the coil spring by considering the time-varying vibration load, i.e., root mean square (rms) varies with time and the uncertainties of geometric parameters. First, a synthetic method for time-varying vibration loads is proposed. The time-varying load is decomposed into multiple stationary Gaussian short samples represented by their power spectral density (PSD). These PSDs are synthesized according to the distribution characteristics of spectral values, in which data that are non-Gaussian are processed with the Johnson system. Second, the influence of parameter uncertainties in the coil spring is studied by a Monte Carlo analysis of the stress frequency response function. Finally, the fatigue life is calculated and compared with the results predicted by using the measured stress. The results show that the synthetic spectrum has almost the same damage potential as the measured time-varying load. In comparison with results predicted from the measured stress, the synthetic spectrum gives much better estimates of the fatigue life of the coil spring than the average spectrum. Parameter uncertainties of coil springs significantly affect fatigue life and should be taken into account.

Keywords: Railway vehicle; Coil spring; Time-varying vibration load; Synthetic spectrum; Parameter uncertainty; Fatigue life.

1 Introduction

Railway vehicles are fitted with two levels of the suspension system to reduce the vibration transmission from the wheel/rail excitation to the car body, thereby improving the ride quality [1]. The primary suspension is located immediately above the axle boxes of the wheelsets and is often formed of steel coil springs; the secondary suspension connects the bogie frame with the car body and is commonly uses air-springs. Recently, however, fatigue fractures of coil springs in the primary suspension have been found to occur frequently for different kinds of railway vehicles in service, including high-speed trains, locomotives and metro vehicles [2-4]. Also, according to the statistics of the fractures of coil springs within a metro train, the service life of fractured coil springs varies within a wide range (0.2 million km ~ 1 million km). Examples of fractured springs are shown in Figure 1.

Figure 1. Examples of fractured coil springs.

Currently, coil springs are generally designed using Goodman diagrams based on the EN 13906 standard [5] to assess their durability. However, recent research results [2-4] show that the EN 13906 standard cannot consider the internal resonances within coil springs, which are significant for fatigue life. In these researches the vibration load of coil springs is regarded as a stationary Gaussian load and expressed by its power spectral density (PSD), from which the stress response PSD is obtained by combining it with the structural dynamic properties in the form of a stress frequency response function (FRF). This allows a more accurate estimate of the fatigue life with the

frequency method [6,7], compared with that obtained by using the EN 13906 standard.

However, there are two shortcomings in these fatigue life evaluation methods. The first is that it is not appropriate for the vibration load to be assumed to be stationary and Gaussian. The vibration acceleration of the axle box excited directly by the wheel/rail interaction is generally regarded as the vibration load for the coil spring [3,4]. During the service period of railway vehicles, different track types [8], evolving wheel/rail contact surface conditions [9] and different operating modes result in complex and changing wheel/rail forces. It leads to the time-varying vibration load of coil springs, that its rms varies with time, which is non-stationary and non-Gaussian [10]. If this is not taken into account, the evaluated fatigue damage will be less than the damage occurring in practice [11,12]. The other shortcoming is that the fatigue life is generally obtained as a deterministic value, whereas the fatigue life of fractured coil springs is found to vary within a wide range. Narayanan [13] and Dodwell [14] show that such variations in the fatigue life of structures are mainly caused by uncertainties in structural parameters. Therefore, to obtain a reasonable fatigue life estimate of the coil springs, both the time-varying vibration load and the uncertainties of structural parameters should be considered.

The use of time domain methods to assess the fatigue life of structures subjected to time-varying loads requires considerable computing resources [6]. In contrast, the frequency domain method can provide rapid calculations of fatigue damage, but cannot be directly applied to time-varying loads. A number of recent investigations have considered the use of frequency domain methods for fatigue life prediction of structures exposed to time-varying loads. Li and Ince [15] assessed the structural fatigue damage under time-varying loads by discretizing the evolutionary PSD [16]. Trapp and Wolfsteiner [11] decomposed the characterization of the varying loads into stationary Gaussian portions with the non-stationary matrix method, which allows the direct use of the frequency domain method for fatigue life prediction. Zorman et al. [17] combined short-time narrowband spectra with the structural dynamic characteristics to assess the structural damage under non-stationary loads. However, each of these methods has the

disadvantages of complicated calculation processes and a large amount of calculation. In contrast, the MIL-STD-810G standard et al. [18] proposed a synthetic method to quickly obtain an equivalent spectrum for multiple stationary and Gaussian vibration loads. While this method cannot be directly used to synthetic the time-varying vibration load that is non-Gaussian. For this, You et al. [19] synthesizes the time-varying loads of railway vehicles by using the Johnson system [20], which allows the transformation of non-Gaussian data to Gaussian data. However, the correlation between mean value and variance used to obtain the value of the synthetic spectrum is ignored in [19].

The dynamic properties of coil springs are determined by their material and geometric parameters [21]. Due to tolerances in manufacturing and installation, however, these parameters are uncertain and lead to variability in the dynamic characteristics and fatigue life of the coil springs. The influence of parameter uncertainties on the dynamic characteristics can be obtained by the Monte Carlo (MC) simulation method [13-14,22]. In MC simulation, a large number of simulations are performed and used to determine the statistical distribution of the dynamic response. The input parameters are chosen from a random distribution of uncertain parameters described according to their probability density function (PDF). Therefore, the MC method has the advantages of a simple calculation process and effective calculation results. In the present context, it is suitable for determining the dynamic characteristics of coil springs, such as the stress FRF, taking account of uncertainties in input parameters.

This paper aims to provide a method for fatigue life estimation of coil springs within the primary suspension of railway vehicles, taking into account both the time-varying vibration load and the uncertainties of structural parameters. The paper is organized as follows. In Section 2, the synthetic method for approximating the time-varying vibration load is proposed. In Section 3, the synthetic spectrum for fatigue analysis of coil springs is generated that takes account of the non-stationary, non-Gaussian characteristics of time-varying loads. The statistical distribution of the stress FRFs of the coil spring is obtained with the MC method in Section 4. These results are

used to calculate the fatigue life in Section 5, and then the proposed method is verified with experimental data in Section 6. The conclusions are summarized in Section 7.

2 Synthetic method for approximating time-varying vibration load

The coil spring is subjected to time-varying vibration loads in service [10,11]. To allow for this in a frequency domain method for the fatigue analysis, a PSD is generated that has almost equal damage potential to the actual time-varying vibration load. This PSD is called a synthetic spectrum. The method to generate the synthetic spectrum is described in this Section.

2.1 Synthetic method

(1) PSD estimation of vibration load

The time-varying vibration load is first decomposed into many short samples of equal time length T which can be considered to be weakly stationary [10]. The PSD of a stationary vibration load can be estimated by:

$$G_k(f) = \frac{2}{T}\left|X_k(f)\right|^2 \tag{1}$$

where $G_k(f)$ is the one-sided PSD at frequency f; k represents the index of the spectral line (k = 1, 2, …, N); $f = k\,\Delta f$, where Δf represents the frequency interval; $X_k(f)$ is the k^{th} spectral line of the Fourier transform. X_k is a complex number with real part X_{kR} and imaginary part X_{kI}; these can be considered as uncorrelated Gaussian random variables with equal variance and zero mean [23], X_{kR}, $X_{kI} \sim N(0, \sigma^2)$.

Assuming that the PSD estimate of the stationary load is unbiased, the true value of the PSD $\bar{G}_k(f)$ at frequency f can be expressed as follows:

$$\bar{G}_k(f) = E(G_k(f)) = \frac{2}{n_d T}\sum_{m=1}^{n_d} E\left(\left|X_k{}^m\right|^2\right) \tag{2}$$

where the index m = 1, 2, …, n_d is used to indicate the individual segment data for a stationary load; E represents the line average. To find the statistical distribution of the PSD estimates at frequency f, they can be written as:

$$\frac{G_k(f)}{\bar{G}_k(f)}=\frac{|X_k|^2}{E(|X_k|^2)}=\frac{X_{kR}{}^2+X_{kI}{}^2}{E(X_{kR}{}^2+X_{kI}{}^2)}=\frac{X_{kR}{}^2+X_{kI}{}^2}{2\sigma^2}=\frac{1}{2}\left[\left(\frac{X_{kR}}{\sigma}\right)^2+\left(\frac{X_{kI}}{\sigma}\right)^2\right] \tag{3}$$

The bracket on the right-hand side of Eq. (3) contains the squared sum of two variables with Gaussian distribution, which conforms to the chi-squared distribution with two degrees of freedom (DOFs). If the PSD estimate in Eq. (2) is based on an average of n_d samples,

$$\frac{2n_dG_k(f)}{\bar{G}_k(f)}\sim\chi^2(2n_d) \tag{4}$$

If the number of DOFs $2n_d$ is greater than 30, the chi-squared distribution can be approximated as Gaussian, $\sqrt{2\chi^2(2n_d)}\sim N(\sqrt{2n_d-1},1)$ [23]. Therefore, when the PSD estimation is based on an average of at least 15 samples, the square root of the PSD at each frequency approximately follows a Gaussian distribution. It indicates that the short sample should be decomposed into at least 15 samples greater than 1 s. Therefore, the time length T for short sample is 20 s in this paper.

(2) Upper normal tolerance limit

For a set of PSDs for many short samples, if the square roots of PSDs at the k^{th} spectral line ($\sqrt{G_k}$) follow the Gaussian distribution, the upper normal tolerance limit (NTL) can be estimated which exceeds a proportion β of the samples with a certain confidence coefficient α.

$$\begin{gathered}P(F\le\hat{F})=\alpha\\ F=\mu+Z_\beta\sigma;\ \ \hat{F}=\hat{\mu}+K\hat{S}\end{gathered} \tag{5}$$

where F and $\hat{F}$ represent the true and estimated upper NTL for $\sqrt{G_k}$ corresponding to the proportion β; Z_β represents the β quantile of the Gaussian distribution; $\hat{\mu}$ and $\hat{S}$ represent the mean and variance for $\sqrt{G_k}$. It can be seen that the mean and variance should be treated as a whole to estimate the $\hat{F}$, but they are regarded as independent in [19]. Essentially, the NTL method involves interval estimation of the true upper limit

F, resulting in a one-sided confidence interval.

The estimates $\hat{F}$ can be obtained by solving for the coefficient *K*. Rearranging the inequality in brackets in Eq. (5).

$$\frac{\mu - \hat{\mu} + Z_\beta \sigma}{\hat{S}} \le K \tag{6}$$

Multiplying both sides of Eq. (6) by the square root of the sample size *M* (the number of PSDs), and then dividing the numerator and denominator on the left of the inequality by σ, yields:

$$\frac{\frac{\mu - \hat{\mu}}{\sigma / \sqrt{M}} + Z_\beta \sqrt{M}}{\hat{S} / \sigma} \le K\sqrt{M} \tag{7}$$

According to statistical theory [23], the distribution of portion of the left-hand side of Eq. (7) is

$$\begin{cases} \dfrac{\mu - \hat{\mu}}{\sigma / \sqrt{M}} \sim N(0,1) \\ \dfrac{(M-1)\hat{S}^2}{\sigma^2} \sim \chi^2(M-1) \end{cases} \tag{8}$$

from which the distribution of the left-hand side of Eq. (7) is

$$\frac{\frac{\mu - \hat{\mu}}{\sigma / \sqrt{M}} + Z_\beta \sqrt{M}}{\hat{S} / \sigma} \sim t_\alpha (M-1, Z_\beta \sqrt{M}) \tag{9}$$

Therefore, the left-hand side of Eq. (7) follows the non-central *t* distribution with *M*–1 DOFs and non-central parameter $Z_\beta \sqrt{M}$. Then, the value of the synthetic spectrum at the k^{th} spectral line $\tilde{G}_k$ can be expressed as follows:

$$\tilde{G}_k = \hat{F}^2 \tag{10}$$

where $\hat{F}$ is given by

$$\hat{F} = \hat{\mu} + K_{M,\alpha,\beta}\hat{S}$$
$$K_{M,\alpha,\beta} = \frac{t_\alpha(M-1, Z_\beta\sqrt{M})}{\sqrt{M}} \tag{11}$$

(3) Upper limit for non-Gaussian data

Eq. (10) is only applicable for Gaussian data. However, in general for vibration loads of the railway vehicle, the distribution of the values $\sqrt{G_k}$ is non-Gaussian, which is tested with the quantile-quantile plot (Q-Q plot) [23]. Therefore, to calculate the upper limit of non-Gaussian data based on the proportion β, the data is first mapped onto a Gaussian data set based on the families of distribution functions of the Johnson system [20]. These can be written as

$$z = \gamma + \eta k_i\left(x;\lambda,\varepsilon\right) \tag{12a}$$

$$k_i\left(x,\lambda,\varepsilon\right) = \begin{cases} \sinh^{-1}\left(\dfrac{x-\varepsilon}{\lambda}\right), i=1 \\ \ln\left(x-\varepsilon\right), i=2 \\ \ln\left(\dfrac{x-\varepsilon}{\lambda+\varepsilon-x}\right), i=3 \end{cases} \tag{12b}$$

Here z represents the standard Gaussian data; x the non-Gaussian data; γ, η, λ, and ε are parameters of the Johnson system (Appendix A); i depends on the quantiles (x_1, x_2, x_3, x_4) for x.

$$\begin{cases} m = x_4 - x_3 \\ n = x_2 - x_1 \\ p = x_3 - x_2 \end{cases} \tag{13}$$

when $mn/p>1$, $i = 1$; when $mn/p = 1$, $i = 2$; and when $mn/p < 1$, $i = 3$.

The true upper limit value F_z, based on the proportion β, of the standard Gaussian data z can be obtained with $\mu = 0$, $\sigma = 1$:

$$F_z = \mu + z_\beta\sigma = z_\beta \tag{14}$$

This value of F_z is then substituted into Eq. (12a) to allow indirect calculation of the upper limit $\hat{F}_v$ of the non-Gaussian data based on the proportion β:

$$F_z = \gamma + \eta k_i\left(\hat{F}_v;\lambda,\varepsilon\right) \tag{15}$$

From this, the square of $\hat{F}_v$ is value of the synthetic spectrum.

2.2 Application of the synthetic method

The flowchart of the process for generating the synthetic spectrum of time-varying vibration loads is shown in Figure 2.

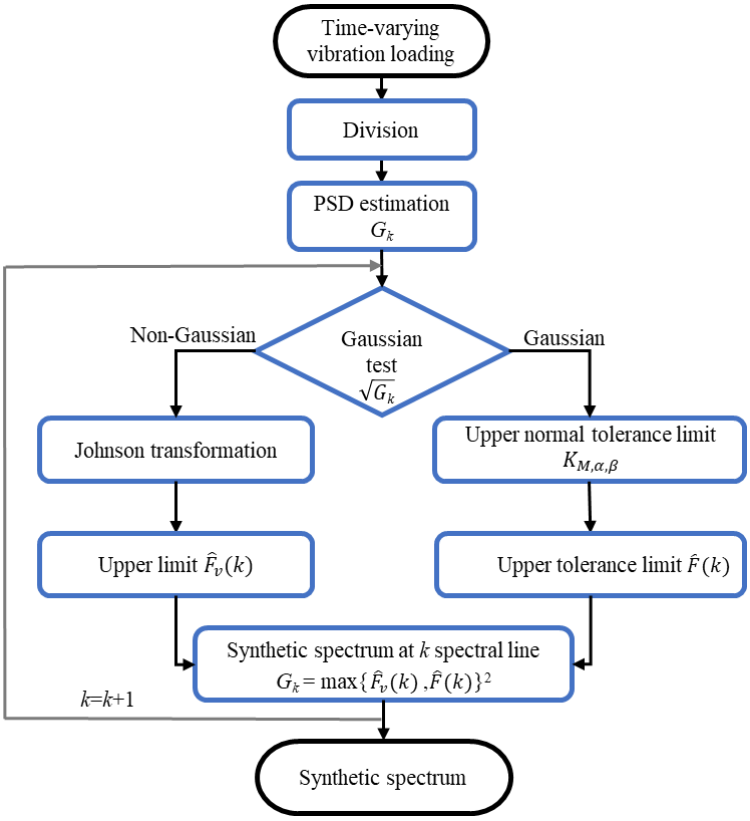

Figure 2. Process for generating synthetic spectrum of time-varying vibration load.

To illustrate the synthetic method, example data from measurement (mission profile 1 shown in Figure 5) are used to calculate the synthetic spectrum for time-varying loads. Here, the value of the synthetic spectrum is calculated at one frequency (60 Hz) by way of an example. The calculation at other frequencies follows the same process.

The synthetic process is as follows:

(1) Division of time-varying load: the example data (of total length 3250 s) is decomposed into many short samples of equal length (20 s), and the PSD of each short

sample $G_k(f)$ is calculated.

(2) PDF estimation of $\sqrt{G_k}$: if the values of $\sqrt{G_k}$ are Gaussian, the value of the synthetic spectrum at frequency f can be directly obtained with Eq. (10); otherwise, the values of $\sqrt{G_k}$ will be transformed into Gaussian data with the Johnson system, Eq. (12). As shown in Figure 3(a), the square roots of the PSDs at 60 Hz are non-Gaussian, which is tested with the QQ plot.

(3) Transformation of non-Gaussian data [20]:

a) An empirical value Z is selected according to the sample size and the probabilities (P_{-3Z}, P_{-Z}, P_Z, P_{3Z}) are determined corresponding to the quantiles ($-3Z$, $-Z$, Z, $3Z$) according to the standard Gaussian distribution table. Supposing that $Z = 0.524$ is chosen, the probabilities of the quantiles are (5.8%, 30%, 70%, 94.2%).

b) The quantiles (x_1, x_2, x_3, x_4) of the non-Gaussian data are determined according to the probabilities (P_{-3Z}, P_{-Z}, P_Z, P_{3Z}). Specifically, the non-Gaussian data consisting of n samples are sorted from smallest to largest to form a new sequence X. The numbers in the sequence X corresponding to these probabilities are $i_{-3Z} = nP_{-3Z} + 1/2$, etc; thus, $(x_1, x_2, x_3, x_4) = (X_{i_{-3Z}}, X_{i_{-Z}}, X_{i_Z}, X_{i_{3Z}})$. For the non-Gaussian example data, (x_1, x_2, x_3, x_4) = (0.016, 0.13, 0.54, 1.85).

c) The values (x_1, x_2, x_3, x_4) are used to determine the value of i. In the example, $mn/p = 0.87$ and the distribution function $k_3(x, \lambda, \varepsilon)$ is selected. It substituted into Eq. (12a) to convert the non-Gaussian data into standard Gaussian data as shown in Figure 3(b).

$$z = \gamma + \eta \ln\left(\frac{x-\varepsilon}{\lambda+\varepsilon-x}\right) = 2.74 + 0.77 \times \ln\left(\frac{x+0.023}{10.33-0.023-x}\right) \tag{16}$$

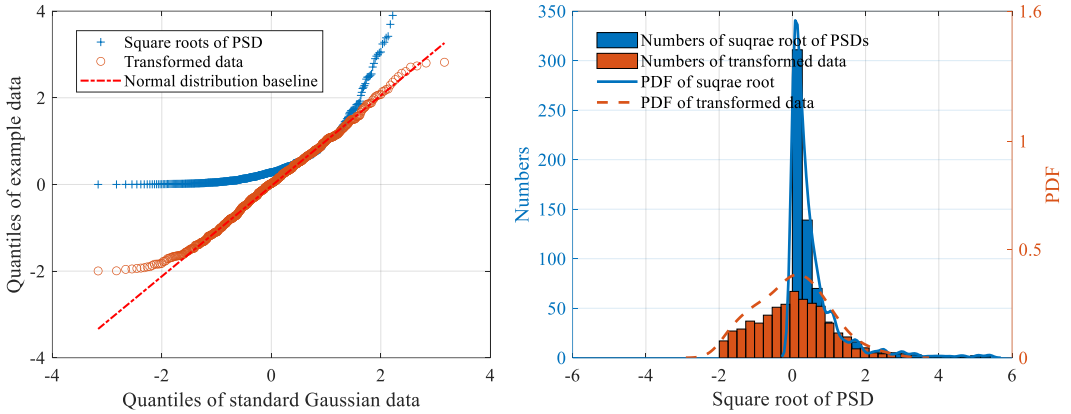

(a) (b)

Figure 3. Transformation of non-Gaussian data. (a) Quantile-quantile plot of example data versus standard Gaussian distribution data; (b) distribution characteristics of square roots of PSDs

(4) Calculation of synthetic spectrum: The upper limit value of the non-Gaussian data can be calculated by Eq. (15), and the square of this value is the synthetic PSD. For the non-Gaussian example data, if these data were assumed to be Gaussian in step (2), the value of the synthetic spectrum would be 2.45 derived with the NTL method (β = 90%), whereas, derived with the Johnson system this value is 4.0. This indicates the potential errors of using the conventional NTL method with non-Gaussian data.

3 Synthetic spectrum for fatigue analysis of coil springs

3.1 Measurements for time-varying vibration load of coil springs

Measurements have been carried out on a metro train with a maximum running speed of 80 km/h. The primary suspension, shown in Figure 4, consists of two concentric coil springs mounted directly above the axle box and a vertical damper which is offset to one side. The coil springs within the primary suspension are excited at their lower end by the vibration of the axle box, whilst the upper end can be considered as approximately fixed due to the connection to the bogie frame. An accelerometer was therefore installed on the axle box, and used to obtain the vertical vibration which can be used to represent the time-varying load of the coil spring. A strain gauge rosette was attached to the outer coil spring at a distance of 1.2 circles from the lower end, on the inside face. This is used to obtain the dynamic strain, which will be used to verify the proposed method in Section 6. The installation of the sensors is

shown in Figure 4.

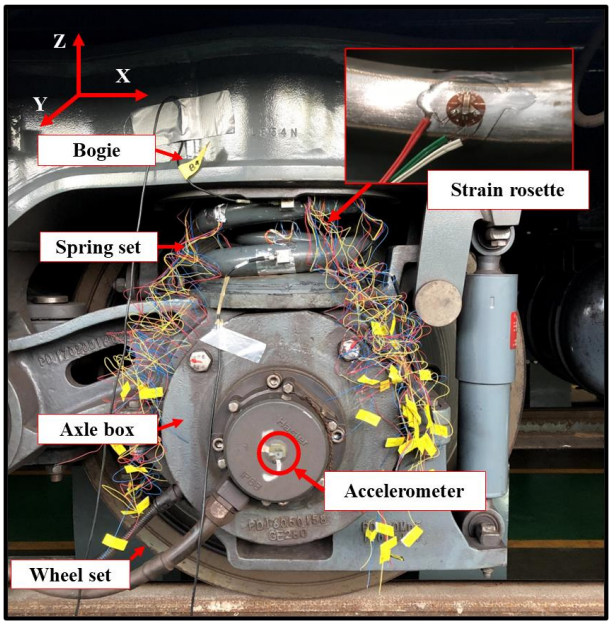

Figure 4. The installations of strain gauge rosette and accelerometer in the field test.

The vibration load of the coil spring in service is time-varying (i.e., rms varies with time) due to the evolving wheel/rail contact surface conditions and different operating speeds. However, to simplify the analysis, it can be assumed that the wheel/rail surface conditions are regularly maintained, resulting in a periodic change of the vibration load. Therefore, it is sufficient to determine the evolution of vibration load in one maintenance cycle (0.15 million km for this metro system). To this end, four mission profiles of vibration loads within a maintenance cycle were measured over the whole route, as shown in Figure 5.

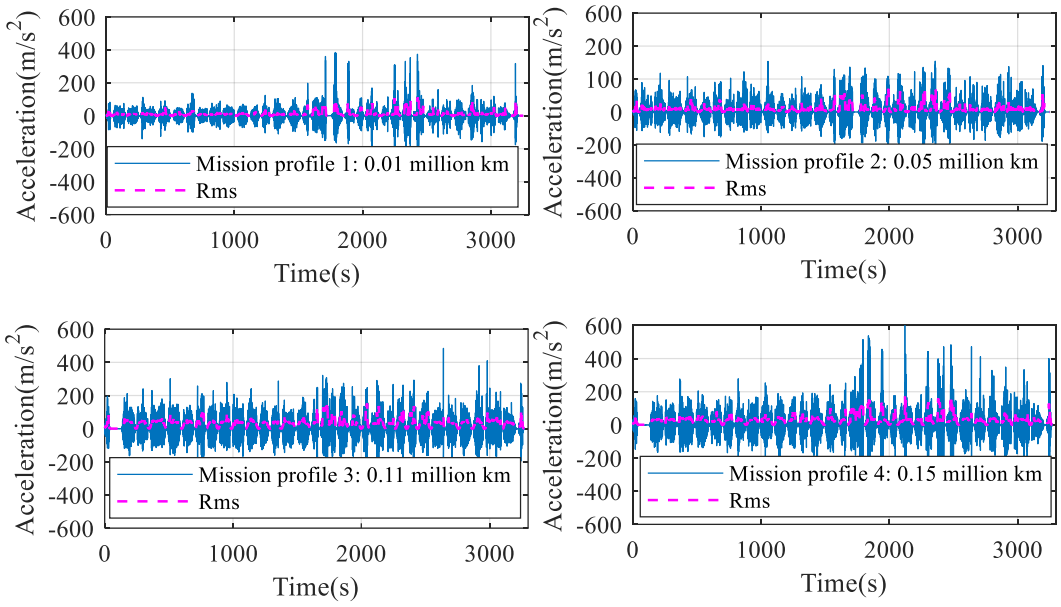

Figure 5. Four measurements of time-varying vibration loads over a maintenance cycle.

3.2 Synthetic spectrum

High instantaneous vibration intensities have an enormous effect on the fatigue failure of a structure [11,24-25]. Moreover, according to the previous studies [26], the structure designed based on the 90% quantile of time-varying vibration loads has high reliability. Thus, the synthetic spectrum for the time-varying vibration load of the coil spring is obtained with $\beta = 90\%$ and $\alpha = 95\%$.

To illustrate this, Figure 6 shows the PSDs of the individual short samples for the four mission profiles. The average spectra are shown as the thick dotted lines and the synthetic spectra based on the above criteria are shown as the solid lines.

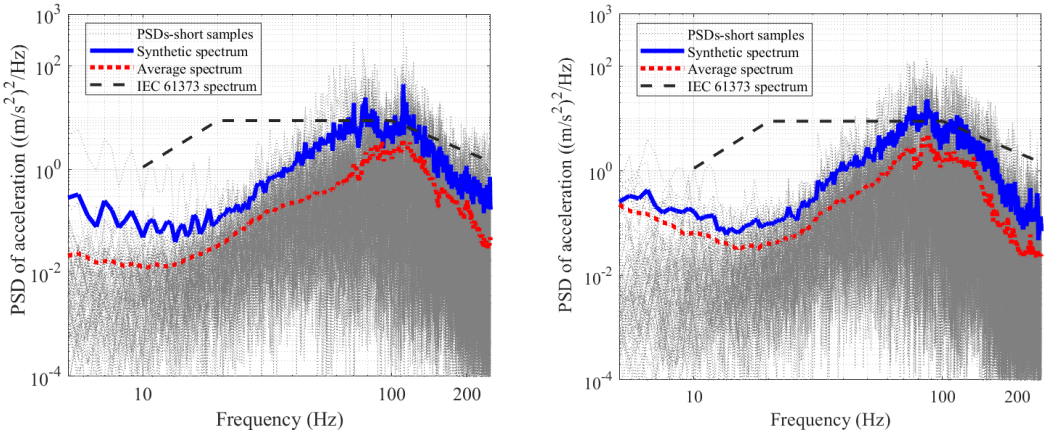

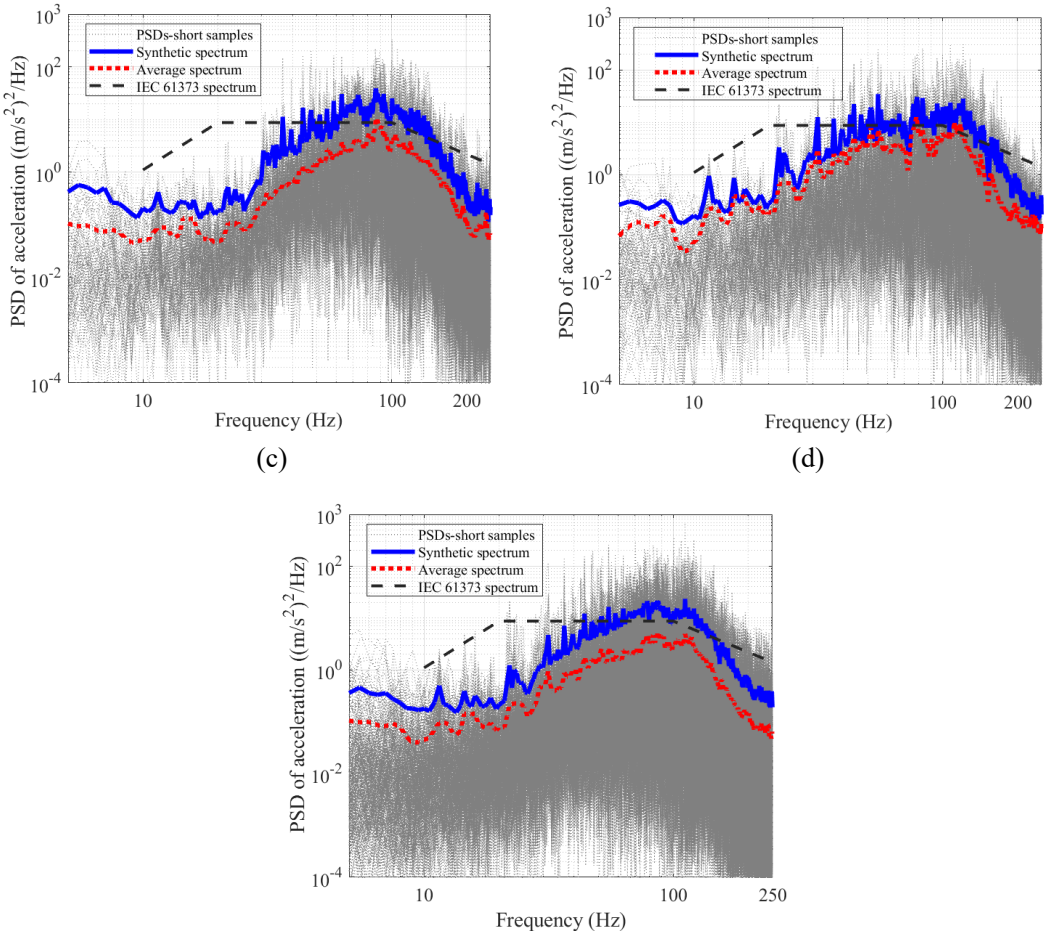

Figure 6. Synthetic spectrum of time-varying vibration loads for (a) mission profile 1; (b) mission profile 2; (c) mission profile 3; (d) mission profile 4; (e) the four mission profiles as a whole.

In Figure 6, significant variations can be seen between the individual short samples and differences can also be seen between the mean spectra of the different mission profiles, which indicates the time-varying nature of vibration loads. The average spectrum and the synthetic spectrum have consistent shapes. However, the average spectrum amplitude is lower than that of the synthetic spectrum, which is based on β = 90%. Thus, the synthetic spectrum contains higher vibration amplitudes.

For comparison, the standard vibration PSD from the IEC 61373 standard [27] for the area around the axle box of a railway vehicle is also presented. This is intended as a spectrum for testing train-mounted equipment and is based on measured vibration acceleration data. However, compared with this standard spectrum, the synthetic spectrum has a different shape, emphasizing the frequency components between 60 and 130 Hz. This spectrum is more suitable for characterizing the frequency domain

characteristics of the time-varying vibration load on this particular metro. The peak frequencies between 60 and 130 Hz can be identified as the main frequency range of the fatigue load for the coil spring in service.

4 Dynamic properties of coil spring with uncertainties

4.1 Finite element model

As shown in Figure 7, a finite element (FE) model has been established for the primary suspension and bogie frame to analyse the structural dynamic properties of the installed coil spring. As the secondary suspension is very soft, it isolates the car body at frequencies above a few Hz; the car body is therefore represented simply by a single mass element that is connected to the bogie frame through spring/damper elements. The bogie frame and the primary suspension springs are discretised by solid tetrahedral elements, and the upper ends of the spring sets are coupled to the bogie frame. The rotary arm rubber bearing is modelled with spring elements and the hydraulic dampers within the primary suspension are modelled with damping elements. The parameters of railway vehicle suspension and the coil spring set are presented in Table 1 and Table 2.

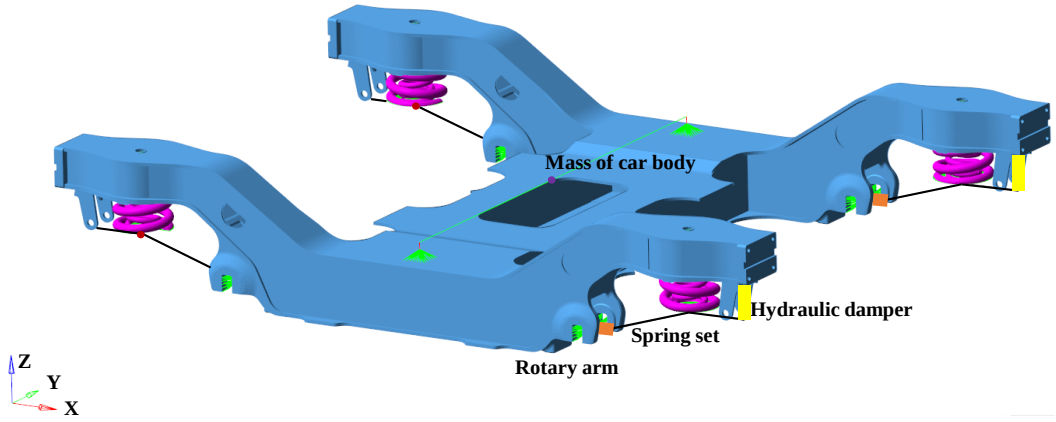

Figure 7. The finite element model of the primary suspension and bogie frame.

Table 1. Vehicle parameters

Description	Value	Unit
Half of car body mass	18000	kg
Vertical stiffness of secondary suspension (per side)	0.3×10^6	N/m
Vertical damping coefficient of hydraulic damper within secondary suspension (per side)	20×10^3	N.s/m
Radial stiffness of rotary arm rubber bearing	8×10^6	N/m
Transverse stiffness of rotary arm rubber bearing	6×10^6	N/m
Vertical damping coefficient of hydraulic damper within primary suspension	15×10^3	N.s/m

Table 2. Design parameters of the coil spring set

Parameter	Outer	Inner	Unit
Number of active coils *n*	3.8	6.8	
Wire diameter *d*	38	24	mm
Spring diameter *D*	204	120	mm
Free height	312	312	mm
Shear modulus	78.5×10^9		Pa
Density	7950		kg/m^3
Poisson's ratio	0.3		

First, a modal analysis is carried out on the outer coil springs. The lower ends of the coil springs in the finite element model are fully constrained. The modes are identical for all four coil springs so results are only presented for one. For verification, a modal experiment was conducted on the outer coil spring in situ. Twenty accelerometers were attached on the coils at equal intervals and the spring was excited using an impact hammer. The first three natural frequencies and mode shapes of the coil spring obtained from the FE model and the measurement are compared in Figure 8. The results from the numerical model agree well with the measurement, with differences in natural frequency of less than 2 Hz and similar mode shapes. These results give confidence in using the FE model to predict the fatigue life of the coil springs.

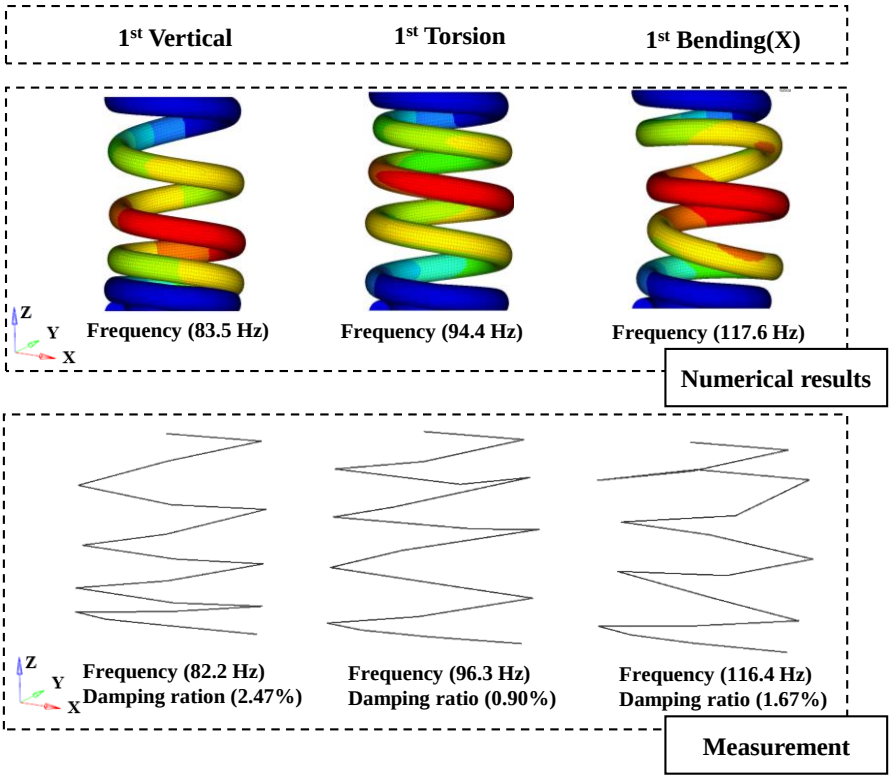

Figure 8. Comparison of modal results from the FE model and measurement.

4.2 Stress FRF of coil spring

To calculate the stress distribution in the coil spring, the modal damping ratio from the modal experiment is used in the FE model. Meanwhile, for the modal damping ratio at modal frequencies of the bogie frame, this value is set as an empirical value of 2%. The lower ends of the coil springs are constrained except in the vertical direction and a unit vertical acceleration at each frequency, is applied to this lower end. The stress due to this unit acceleration is calculated as an FRF; this is shown in Figure 9 for two locations on the coil spring.

For the first principal stress, the maximum stress FRF is located at 0.75 circles from the lower end, which is at the transition between the active coils (that are free to move) and the support coils (that are in contact with the bearing surface). In the measurements described in Section 2, the strain gauges could not be installed here because of the contact between the spring and the support surface. Thus, a position was selected at 1.2 circles from the lower end on the inside face; this has an FRF with a smaller magnitude. The peak frequencies of the FRFs at these two positions correspond

to the first vertical mode (83.5 Hz), the first bending mode (116 Hz), and the second vertical mode (157 Hz). The peak value at the first vertical mode is more than five times larger than that at the other two modes.

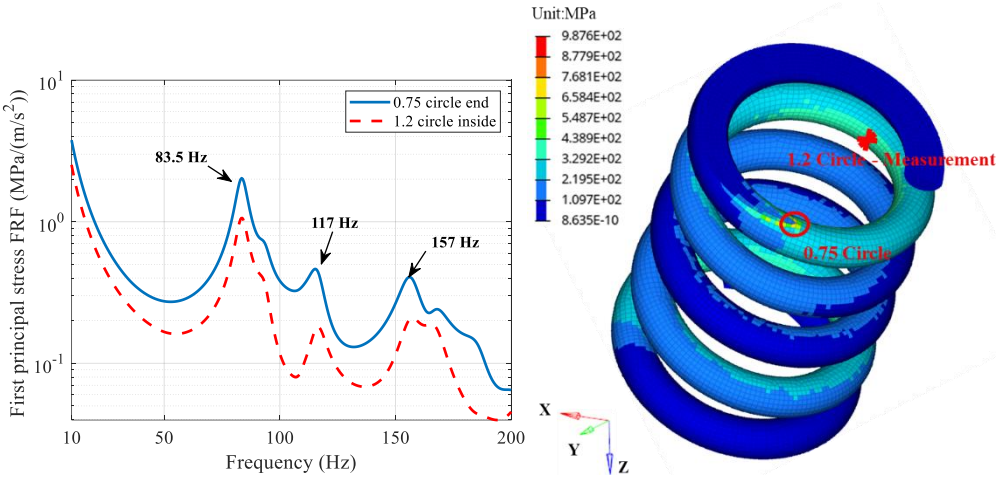

(a) (b)

Figure 9. Stress FRF. (a) FRF of the first principal stress; (b) stress distribution contour at the first vertical mode (83.5 Hz), viewed from the bottom.

4.3 Variation in stress FRF

In this section, the influence of uncertainties in the geometric parameters (number of active coils n, spring diameter D, wire diameter d) on the stress FRF is studied by using the MC method, assuming that the material properties can be considered to be constant. According to the hypothesis presented in [28], n, d, and D can be assumed to conform to independent normal distributions, in which the mean values are the nominal design values and the standard deviation is obtained from the manufacturing tolerance Δu according to the '3σ' law.

$$\sigma = \frac{|\Delta u|}{3} \tag{17}$$

The manufacturing tolerances of n, d, and D are ±0.5, ±0.5 mm, and ±2.04 mm.

Considering the computational costs, 100 simulations are performed with the MC method to determine the variability of the stress FRFs of the coil spring. For each simulation, the stress FRF curves in the vicinity of the modal frequencies are shown in Figure 10 at the 0.75 and 1.2 circle positions. Individual results are highlighted for the

sets of geometric parameters corresponding to the minimum and maximum lifetime of the coil spring (as described in Section 5).

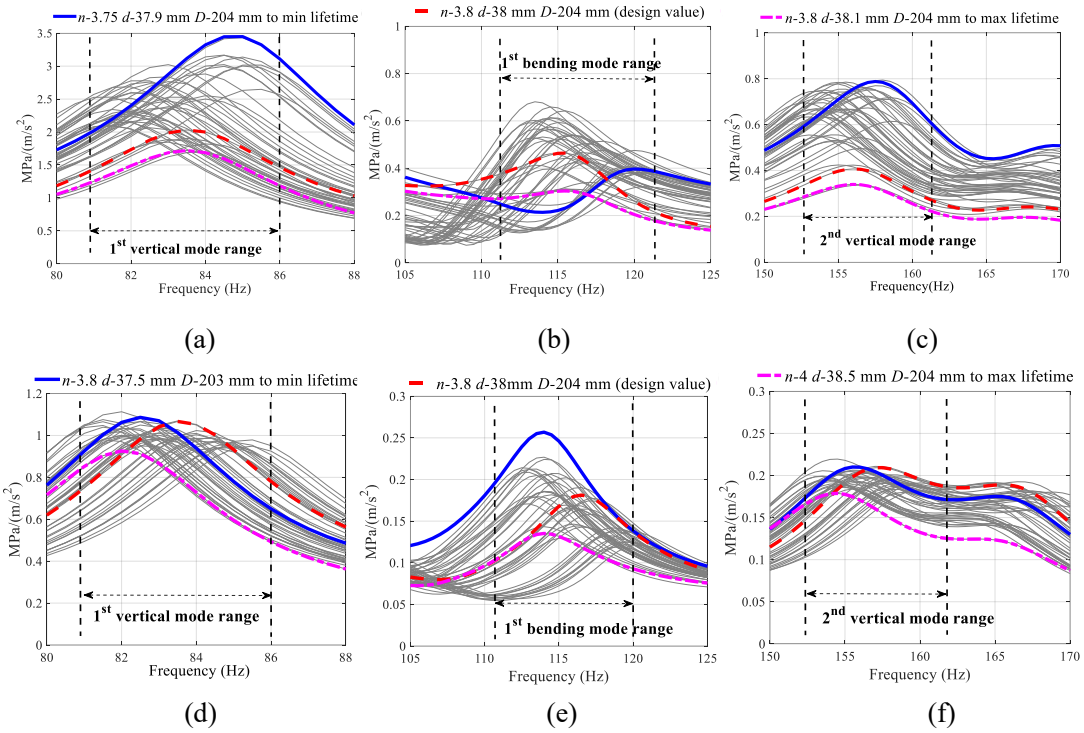

Figure 10. Variation range of the stress FRF at the 0.75 circle position: (a) the 1st vertical mode; (b) the 1st bending mode; (c) the 2nd vertical mode. At the 1.2 circle inside position: (d) the 1st vertical mode; (e) the 1st bending mode; (f) the 2nd vertical mode. The red curve corresponds to the design parameters, the blue curve to the minimum fatigue life and the pink curve to the maximum fatigue life.

The modal frequency of the first vertical mode with the nominal design parameters is 83.5 Hz. From the different configurations considered, this varies by up to ±3 Hz, between 80.5 Hz and 86 Hz. The maximum value of the stress FRF at the 0.75 circle position varies between 1.6 MPa/(m/s^2) and 3.5 MPa/(m/s^2), compared with 2.0 MPa/(m/s^2) for the nominal parameters; the highest value is 75% greater than the nominal peak value. At the 1.2 circle position the range of maximum amplitudes is smaller and the highest value is only 13% greater than the nominal maximum stress.

5 Fatigue life analysis

For a linear time-invariant system, the stress response PSD $S_\sigma(f)$ can be obtained by [7]:

$$S_\sigma(f) = |H_\sigma(f)|^{2^*} \tilde{G}(f) \tag{18}$$

where $H_\sigma(f)$ is the stress FRF and $\tilde{G}(f)$ is the acceleration load spectrum PSD. In the current method this is the synthetic spectrum.

Fatigue life is generally expressed in terms of an S-N curve, where S represents stress amplitude and N number of cycles. To estimate the fatigue life from a stress PSD, an approximation to the cycle-amplitude distribution is required. For this, Dirlik's method [29] is generally used:

$$P(S_a) = \frac{\frac{D_1}{Q} e^{-\frac{Z_a}{Q}} + \frac{D_2 Z_a}{R^2} e^{-\frac{Z_a^2}{2R^2}} + D_3 Z_a e^{-\frac{Z_a^2}{2}}}{2\sqrt{m_0}} \tag{19a}$$

where $P(S_a)$ represents the PDF of the stress amplitude S_a and Za is the normalized amplitude. The other parameters are defined as:

$$\begin{aligned} &m_i = \int_0^{+\infty} f^i S(f) df;\ Z_a = \frac{S_a}{2\sqrt{m_0}};\ \gamma = \frac{m_0}{\sqrt{m_0 m_2}};\ \chi_m = \frac{m_1}{m_0}\sqrt{\frac{m_2}{m_4}}; \\ &D_1 = \frac{2(\chi_m - \gamma^2)}{1+\gamma^2};\ D_2 = \frac{1-\gamma-D_1+D_1^2}{1-R};\ D_3 = 1 - D_2 - D_1; \\ &Q = \frac{1.25(\gamma - D_3 - D_2 R)}{D_1};\ R = \frac{\gamma - \chi_m - D_1^2}{1-\gamma-D_1+D_1^2}; \end{aligned} \tag{19b}$$

Then the damage $\bar{D}$ of the coil spring per second is evaluated by:

$$\bar{D} = \frac{\nu_p}{C} \int_0^{+\infty} P(S_a) {S_a}^m dS_a \tag{20}$$

where ν_p represents the crossing frequency of stress peaks, $\nu_p = \sqrt{m_4/m_2}$; m and C are parameters of the S-N curve of the coil spring material. The fatigue life X of the coil spring in millions km can be calculated as follows:

$$X = \frac{V}{\bar{D}} / 10^6 \tag{21}$$

where V represents the average running speed of the railway vehicle (8.9 m/s in the current study).

From the 100 stress FRFs calculated in Section 4.2, 100 fatigue life estimates of the coil springs can be obtained. Then the reliability P_s, i.e., the probability of the fatigue life being greater than X, is given as:

$$P_s = P\{g(n,d,D) > X\} = \frac{m_s}{M} \tag{22}$$

where g is the fatigue life result predicted with the synthetic spectrum and Dirlik's method; M=100 is the total number of lifetime estimates, and m_s represents the number of estimates with a fatigue life greater than X.

Figure 11 shows the reliability function P_s of the coil spring calculated for the 0.75 circle position and the 1.2 circle position. A fitted curve is also shown in each graph. Comparing the two graphs, the expected fatigue life based on the stress at the 0.75 circle position is more than 10 times shorter than that based on the 1.2 circle position. Owing to the uncertainties of the geometric parameters, the expected fatigue life of the coil spring based on the stress at the 0.75 circle position can vary between 0.1 and 0.7 million km. This can explain the fact that the service life before springs fracture can vary considerably.

In addition, since the 1st vertical and bending mode frequencies of the coil spring are within the main frequency range of the synthetic spectrum, this caused resonance of the coil spring, resulting in high amplitude vibrations and stresses at these frequencies. It results in the shortest fatigue life of the coil spring less than the overhaul mileage of metro trains (0.6 million km) given by the Chinese standard GB 50157 [30]. This indicates that some measures should be taken to improve the fatigue life of the coil spring, such as ensuring smoother wheel/rail contact surface conditions by shortening the maintenance cycle.

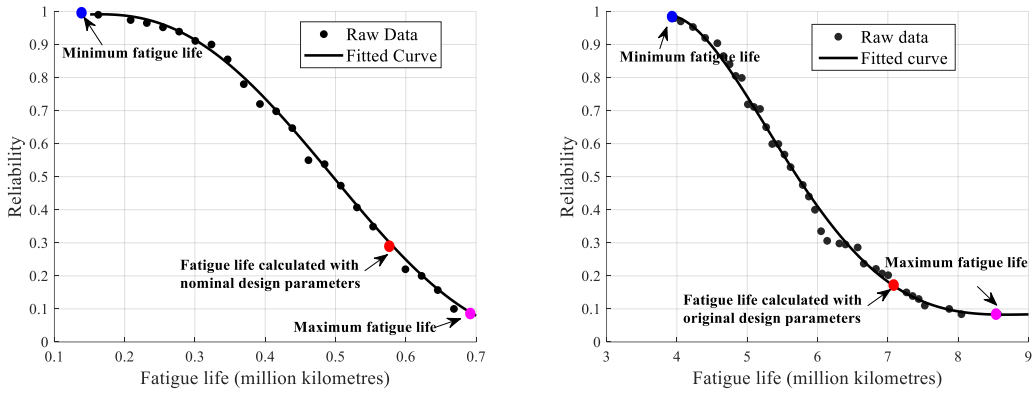

(a) (b)

Figure 11. Fatigue life reliability of the coil spring. (a) 0.75 circle position; (b) 1.2 circle position.

6 Discussion

In order to assess the suitability of the synthetic spectrum in predicting the fatigue life of the coil spring, comparisons are made for each mission profile of the fatigue life predicted by the synthetic spectrum, the average spectrum and the measured stress (determined from the strain measurement). The fatigue life is predicted from the two spectra using the frequency domain method (Eqs (18-22)) for the 100 geometric variants, while the measured stress is used in the time domain method given in Appendix B. In addition, it should be noted that since the strain gauge rosette is attached at the 1.2 circle position of the coil spring, all fatigue life results in this section are predicted based on this position.

The results are shown in Figure 12. In each case the fatigue life, corresponding to 50% reliability, predicted with the synthetic spectrum is between 35% and 65% smaller than that predicted with the measured stress. Conversely, the fatigue life corresponding to 50% reliability predicted with the average spectrum is between 100% and 400% larger than the result from the measured stress.

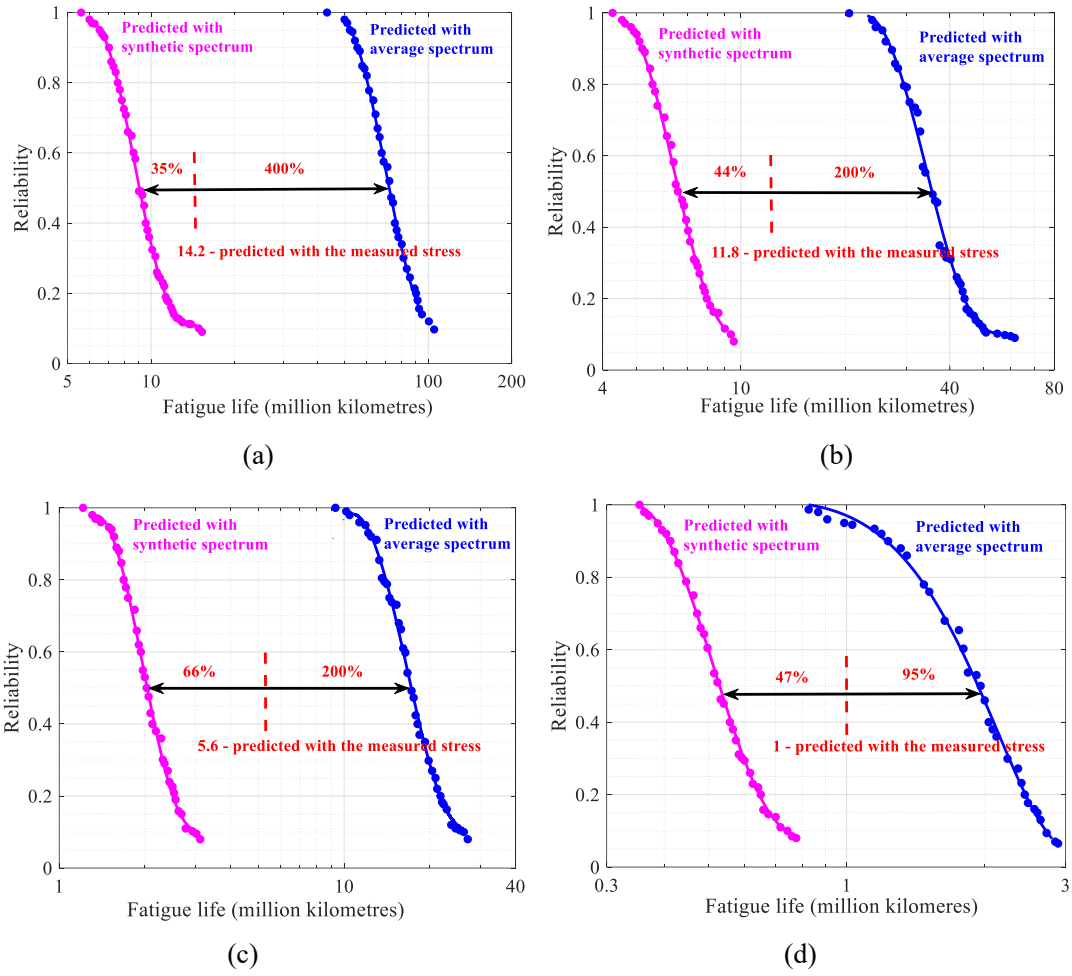

Figure 12. Comparison of fatigue life predicted with different vibration load spectra. (a) Mission profile 1; (b) mission profile 2; (c) mission profile 3; (d) mission profile 4.

According to the Palmgren-Miner rule, fatigue damage is related to the stress amplitude by a power law (Appendix B). This implies that the contribution to the fatigue damage of high stress amplitudes, caused by high amplitudes of vibration loads, is decisive in determining the fatigue life [25]. In the process of predicting fatigue life by the frequency domain method, the average spectrum does not give sufficient weight to high stress amplitudes. Thus, the fatigue life predicted by the average spectrum is significantly longer than that predicted by the measured stress. The synthesised spectrum derived with $\beta = 90\%$ contains more of the high vibration intensities present in the time-varying load, and therefore predicts a fatigue life that is closer to the results obtained with the measured stress.

7 Conclusions

A method is proposed to derive a synthetic load spectrum for use in the fatigue life estimation of coil springs. This method allows the frequency domain approach to be used for fatigue analysis while taking account of the non-stationary and the non-Gaussian character of the vibration load.

The synthetic spectrum contains higher vibration intensities than an average spectrum and has almost the same damage potential as the actual time-varying load. Compared with the average spectrum, the fatigue life of the coil spring estimated with the synthetic spectrum is closer to that determined using the measured stress.

Owing to the uncertainties of the geometric parameters, expressed in terms of their manufacturing tolerances, the expected fatigue life of the coil spring can vary in a wide range (0.1 and 0.7 million km). This highlights that parameter uncertainties have a significant effect on the fatigue life and should be taken into account.

Although the work focuses on coil springs, the proposed fatigue life assessment method proposed is applicable to many other mechanical structures. In addition, there are some limitations in this paper because some parameters were chosen empirically, such as Z in the Johnson system and β. It results in a gap between the fatigue life predicted with the synthetic spectrum and that predicted with the measured data. To solve this problem, a parameters optimization algorithm should be investigated, which is the focus of our future research.

Acknowledgements

This work was supported by the Natural Science Foundation of Shanghai [No. 21ZR1467100], the Shanghai Sailing Program [No. 20YF1451100].

Declaration of Competing Interest

The authors declare that they have no known competing financial interests or personal relationships that could have appeared to influence the work reported in this paper.

Reference

[1] Zhou JS. Vibration and control on railway vehicles. Shanghai: Fudan University Press; 2020. (in Chinese).

[2] Sun WJ, Thompson D, Zhou JS. The influence of vehicle–track dynamic coupling on the fatigue failure of coil springs within the primary suspension of metro vehicles. Veh Syst Dyn. 2020;58(11):1694-1710.

[3] Zhou C, Chi MR, Wen ZF, et al. An investigation of abnormal vibration-induced coil spring failure in metro vehicles. Eng Failure Anal. 2020;108:104238.

[4] Wang KY, Yang YF, Xu MK, et al. An experimental investigation of the mechanism and mitigation measures for the coil spring fracture of a locomotive. Eng Failure Anal. 2022:106157.

[5] British Standards Institution. Cylindrical helical spring made from round wire and bars-calculation and design-Part 1: Compression springs. London: British Standards Institution; 2002. Standard No EN 13906-1:2002.

[6] Liu XX, Zhang YH, Guo HF, et al. Random vibration analysis procedure of railway vehicle. Veh Syst Dyn. 2019;57(4):471-492.

[7] Mršnik M, Slavič J, Boltežar M. Vibration fatigue using modal decomposition. Mech Syst Signal Process. 2018;98(1):548-556.

[8] Ling L, Jiang PB, Wang KY, et al. Dynamic interaction between rail vehicles and vibration-attenuating slab tracks. Constr Build Mater. 2020;258:119454.

[9] Tao GQ, Wen ZF, Liang XR, et al. Measurement and assessment of out-of-round electric locomotive wheels. Proc IMechE Part F: J Rail Rapid Transit 2018; 232(1): 275-287.

[10] Deng CX, Zhou JS, Sun WJ, et al. Analysis of the spectral induction and hierarchical transmissibiliy for railway vehicles' measurement vibration loading. Veh Syst Dyn. 2020;59(10):1587-1606.

[11] Trapp A, Wolfsteiner P. Fatigue assessment of non-stationary random loading in the frequency domain by a quasi-stationary Gaussian approximation. Int J Fatigue. 2021;148:106241.

[12] Palmieri M, Česnik M, Slavič J, et al. Non-Gaussianity and non-stationarity in vibration fatigue. Int J Fatigue. 2017;97:9-19.

[13] Narayanan G, Rezaei K, Nackenhorst U. Fatigue life estimation of aero engine mount structure using Monte Carlo simulation. Int J Fatigue. 2016;83(1):53-58.

[14] Dodwell TJ, Kynaston S, Butler R, et al. Multilevel Monte Carlo simulations of composite structures with uncertain manufacturing defects. Probab Eng Mech. 2021;63:103116.

[15] Li Z, Ince A. A unified frequency domain fatigue damage modeling approach for random-on-random spectrum. Int J Fatigue. 2019;124:123-137.
[16] Priestley M B. Evolutionary spectra and non-stationary processes. Journal of the Royal Statistical Society Series B-Statistical Methodology, 1965, 27:204-237.
[17] Zorman A, Slavič J, Boltežar M. Short-time fatigue-life estimation for non-stationary processes considering structural dynamics. Int J Fatigue. 2021;147: 106178.
[18] US Department of Defense. Environmental Engineering Considerations and Laboratory Tests. USA: Department of Defense; 2019. Standard No MIL-STD-810H:2019.
[19] You TW, Zhou JS, Gong D, et al. Synthesis of random vibration environment spectra for the fatigue analysis and optimization of railway vehicles. Int J Fatigue. 2022;159:106752.
[20] Chou YM, Polansky AM, Mason RL. Transforming Non-Normal Data to Normality in Statistical Process Control. J Qual Technol. 1998;30(2):133-141.
[21] Lee J, Thompson D. Dynamic stiffness formulation, free vibration and wave motion of helical springs. J Sound Vib. 2001;239(2):297–320.
[22] Gregori S, Tur M, José E, et al. Stochastic Monte Carlo simulations of the pantograph–catenary dynamic interaction to allow for uncertainties introduced during catenary installation. Veh Syst Dyn. 2019;57(4):471-492.
[23] Casella G, Berger RL. Statistical inference 2nd Edition. Duxbury: Duxbury Press; 2001.
[24] Karamchandani A, Dalane JI, Bjerager P. Systems reliability of offshore structures including fatigue and extreme wave loading. Int J Fatigue. 1991;4(4):353-379.
[25] D Gong, J Zhou, W Sun. On the resonant vibration of a flexible railway car body and its suppression with a dynamic vibration absorber. J Vib Control 57(1): 1–16.
[26] He XF, Sui FC, Zhai B, et al. Probabilistic and testing analysis for the variability of load spectrum damage in a fleet. Eng Failure Anal. 2013;33:419-429.
[27] International Electro Technical Commission Technical Committee 9. Railway applications-rolling stock equipment-shock and vibration test. Geneva: Standards Press of International Electro Technical Commission; 2010. Standard No IEC 61373:2010.
[28] Zuo SH. Study on fatigue reliability of bolster springs of railway truck bogie. [Master's Thesis]. Beijing: Beijing Jiaotong University; 2010. (in Chinese).
[29] Dirlik T. Application of computers in fatigue analysis. PhD Thesis. University of Warwick; 1985.
[30] Ministry of Housing and Urban-Rural Development of the People's Republic of

China. Code for Design of Metro. Bei Jing: Standards Press of China; 2013. Standard No GB 50157:2013. (in Chinese).

Appendix

Appendix A. Parameters for Johnson system

The parameters of the Johnson system can be expressed as follows [20]:

$$\text{if } i=1,\quad \begin{cases} \eta = \dfrac{2Z}{\cosh^{-1}\left(\left(m+n\right)/2p\right)} \\ \gamma = \eta \sinh^{-1}\left(\dfrac{n-m}{2p\left(mn/p^2-1\right)^{1/2}}\right) \\ \lambda = \dfrac{2p\left(mn/p^2-1\right)^{1/2}}{\left(\left(m+n\right)/p-2\right)\left(\left(m+n\right)/p+2\right)^{1/2}} \\ \varepsilon = \dfrac{x_2+x_3}{2} + \dfrac{n-m}{2\left(\left(m+n\right)/p-2\right)} \end{cases} \tag{A.1}$$

$$\text{if } i=2,\quad \begin{cases} \eta = \dfrac{2Z}{\ln\left(m/p\right)} \\ \gamma = \eta \ln\left(\dfrac{m/p-1}{p\left(m/p\right)^{1/2}}\right) \\ \varepsilon = \dfrac{x_2+x_3}{2} - \dfrac{p\left(m/p+1\right)}{2\left(m/p-1\right)} \end{cases} \tag{A.2}$$

$$\text{if } i=3,\quad \begin{cases} \eta = \dfrac{Z}{\cosh^{-1}\left(\left(1+p/m\right)^{1/2}\left(1+p/n\right)^{1/2}/2\right)} \\ \gamma = \eta \sinh^{-1}\left(\dfrac{\left(p/n-p/m\right)\left(\left(1+p/m\right)\left(1+p/n\right)-4\right)^{1/2}}{2\left(p^2/mn-1\right)}\right) \\ \lambda = \dfrac{p\left(\left(\left(1+p/m\right)\left(1+p/n\right)-2\right)^2-4\right)^{1/2}}{p^2/mn-1} \\ \varepsilon = \dfrac{x_2+x_3}{2} - \dfrac{\lambda}{2} + \dfrac{p\left(p/n-p/m\right)}{2\left(p^2/mn-1\right)} \end{cases} \tag{A.3}$$

where the x_1, x_2, x_3 and x_3 are quantiles of the non-Gaussian data that are determined according to the probabilities; m, n, and p are obtained with Eq. (13).

Appendix B. Fatigue life assessment with the time domain method

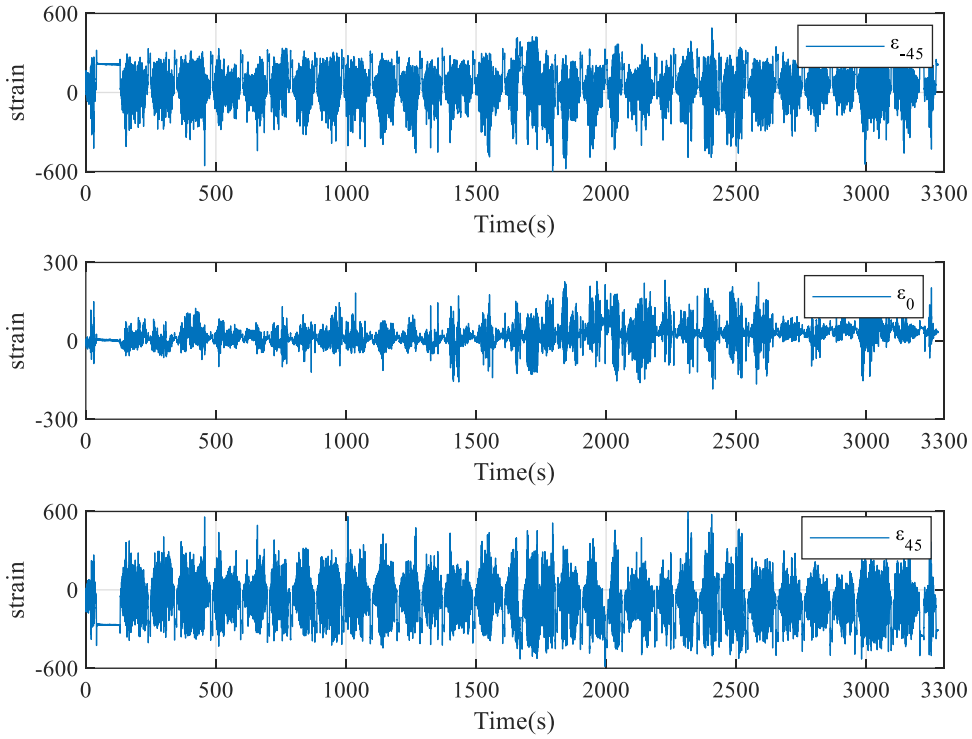

Figure B1. The measured strains from mission profile 1.

The collected strain data, shown in Figure B1 for mission profile 1, can be transformed into the first principal stress σ_1 as:

$$\sigma_1 = \frac{E}{2}\left[\frac{(\varepsilon_{45}+\varepsilon_{-45})}{(1-\mu)} + \frac{1}{(1+\mu)}\sqrt{(\varepsilon_{45}+\varepsilon_{-45})^2+(2\varepsilon_0-\varepsilon_{45}-\varepsilon_{-45})^2}\right] \quad \text{(B.1)}$$

where E is the Young's modulus of the coil spring material; ε_{-45}, ε_0, and ε_{45} are three components of the measured strain; μ is the Poisson's ratio.

The cycles of the first principal stress σ_1 are counted with the rainflow counting method, as shown in Figure B2(a). Based on the S-N curve of the coil spring material (Figure B2(b)), the fatigue damage $\hat{D}$ is calculated with Miner's linear accumulation rule:

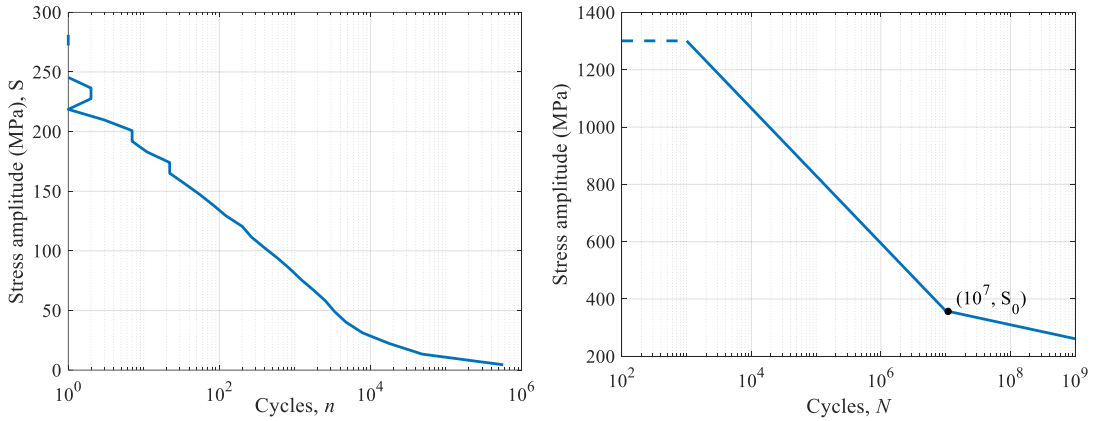

Figure B2. (a) Cycle-amplitude distribution of measured stress; (b) assumed S-N curve of the coil spring material.

$$\hat{D} = \sum \frac{n}{N} = \sum \begin{cases} \frac{n}{10^7} (\frac{S}{S_0})^m, S > S_0 \\ \frac{n}{10^7} (\frac{S}{S_0})^{m+2}, S < S_0 \end{cases} \tag{B.2}$$

where n represents the number of cycles occurring with amplitude S; N represents the number of cycles to fatigue for this stress amplitude; m represents the slope of the S-N curve; and S_0 represents the fatigue limit.

Finally, the fatigue life $\hat{X}$ of coils springs in million km can be predicted by:

$$\hat{X} = \frac{L}{\hat{D}} / 10^6 \tag{B.3}$$

where L is operation mileage in km (38 km for mission profile 1).